Investigation of the Optical and Structural Properties of Cr³⁺-Doped Al₂O₃ and ZnAl₂O₄ Nanoparticles Synthesized by Sol−Gel Method

Ahmed Kadari, Salah Eddine Rezak, Kheira Kassi,
and Mostapha Chehairi

Engineering Physics Laboratory,
Ibn-Khaldoun University of Tiaret,
BP P 78, zaâroura
14000 Tiaret, Algérie

Alumina (Al_2O_3) and spinel zinc aluminate ($ZnAl_2O_4$) nanoparticles were synthesized by a sol−gel method. Pure and chromium (Cr^{3+}) doped Al_2O_3 and $ZnAl_2O_4$ were prepared and then characterized in order to study the influence of chromium doping (impurities) on the physical properties of these compounds. Obtained powders were calcined at 500°C. Optical and structural properties of as-prepared powders were investigated by UV-visible spectroscopy (UV-Vis), Fourier transform infrared spectroscopy (FT-IR) and powder x-ray diffraction (XRD). The band-gap energy values obtained from UV-visible characterization showed the insulator ($E_g = 4.881$ eV) and semi-conductor ($E_g = 3.707$ eV) characters of Al_2O_3 and $ZnAl_2O_4$, respectively. The incorporation of chromium atoms in ours synthesized matrix has been confirmed by the FT-IR spectroscopy; it is explained by the formation of Cr−O complex at 674 cm^{-1} in both materials. The XRD results have shown the crystallographic phases (cubic) of Al_2O_3 and $ZnAl_2O_4$ nanoparticles. The crystallite size was found to be in the range of 192.968 nm to 460.765 nm for Al_2O_3:Cr^{3+}, and it was revealed to be constant (≈ 32 nm) for $ZnAl_2O_4$:Cr^{3+} matrix.

Наночастинки оксиду алюмінію (Al_2O_3) та шпінелі алюмінату цинку ($ZnAl_2O_4$) синтезовано золь−ґель-методом. Чисті та леґовані хромом (Cr^{3+}) Al_2O_3 і $ZnAl_2O_4$ були одержані і потім охарактеризовані з метою вивчення впливу леґування хромом (домішок) на фізичні властивості цих сполук. Одержані порошки прожарювали при 500°C. Оптичні та структурні властивості готових порошків досліджували за допомогою спектроскопії в ультрафіолетовій (УФ) і видимій областях світла (UV-Vis), інфрачервоної спектроскопії з Фур᾿є-перетвором (FT-IR) та порошкової рентґенівської дифракції (XRD). Значення енергії забороненої

зони, одержані за допомогою УФ-видимої-характеризації, показали ізоляторний ($E_g = 4{,}881$ eB) і напівпровідниковий ($E_g = 3{,}707$ eB) характери Al_2O_3 та $ZnAl_2O_4$ відповідно. Втілення атомів Хрому в нашу синтезовану матрицю було підтверджено FT-IR-спектроскопією; це пояснюється утворенням комплексу Cr—O при 674 см$^{-1}$ в обох матеріялах. XRD-результати показали кристалографічні фази (кубічні) наночастинок Al_2O_3 та $ZnAl_2O_4$. Було встановлено, що розмір кристаліту знаходиться в діяпазоні від 192,968 нм до 460,765 нм для Al_2O_3:Cr^{3+}, і було виявлено, що він є постійним (≈ 32 нм) для матриці $ZnAl_2O_4$:Cr^{3+}.

1. INTRODUCTION

Alumina (Al_2O_3) nanoparticles are an excellent ceramic oxide; it has received considerable attention due to their enhanced properties. These kinds of materials are extensively applied in optical industries, electronics, thermoluminescence dosimetry, thermal insulators and in metal cut [1−6]. In addition, these materials are used in catalysts, ceramics, adsorbents, molecular separation, and composite materials [7]. Alumina has different crystallographic phases, in which the γ-Al_2O_3 is the most important phase because of its remarkable properties like high insulation, high strength, high rigidity and transparency [8, 9].

Due to its wide band-gap (≈ 3.8 eV) [10, 11], semi-conducting zinc aluminate $ZnAl_2O_4$ shows increased interest for many applications, such as ultraviolet photoelectronic devices, sensors, high-temperature material, optical coating and catalysts or supports in many catalytic reactions due to its high thermal stability, low surface acidity and hydrophobicity properties [12−14]. It has the chemical formula of AB_2O_4, where A stands for metal cation, which occupies a tetrahedral site, and B represents Al, which occupies the octahedral sites, within the cubic packed crystal structure that belongs to the space group $Fd3m$ [14, 15].

Recently, different physical and chemical preparation techniques, such as hydrothermal followed by calcination [16−21], the Pechini process [21], solid-state routes [16], oxalate-precursor co-precipitation [22] and the spray pyrolysis method [23], are employed to prepare materials in powders' form composed of nanoparticles. Sol−gel process is one of the effective methods for synthesis of metal-oxide nanoparticles, because it has many advantages than

other methods [24−26]. Transition-metals' ions, such as chromium (Cr^{3+}) and titanium (Ti^{3+}), doped α-Al_2O_3 nanoparticles are known as the most important laser materials; in this context, many studies have been reported on the effects of these impurities on some properties of alumina nanoparticles [27−33]. Alkali, alkaline earth, rare-earth or transition metal ions' doped $ZnAl_2O_4$ have been a subject of several previously published papers, such as referring to europium (Eu^{3+}) ions [34], samarium (Sm^{2+}) ions [35], manganese (Mn^{2+}) ions [14], copper (Cu^{2+}) ions [36], cerium (Ce^{2+}) ions [37], calcium (Ca^{2+}) ions [38] and chromium (Cr^{3+}) ions [10, 11, 39−42].

In the present investigation, the synthesis of alumina (Al_2O_3) and spinel zinc aluminate ($ZnAl_2O_4$) nanoparticles by means of the sol−gel method are described. The effect of chromium (Cr^{3+}) doping on the structural and optical properties has been briefly studied, and the results are discussed. UV-visible spectroscopy (UV-Vis), Fourier transform infrared spectroscopy (FT-IR) and powder x-ray diffraction (XRD) are the techniques used in the characterisation of nanoparticles.

2. MATERIAL AND METHODS

2.1. Material

Each chemical reagent used in the experiment was of analytical grade, and they were used as obtained without further purification. For synthesis, the pure and Cr^{3+}-doped Al_2O_3 and $ZnAl_2O_4$ nanoparticles, aluminium chloride hexahydrate ($AlCl_3 \cdot 6H_2O$, 99% Sigma-Aldrich), aluminium nitrate nonahydrate ($Al(NO_3)_3 \cdot 9H_2O$, 99% Sigma-Aldrich), zinc nitrate hexahydrate ($Zn(NO_3)_2 \cdot 6H_2O$, 99% Sigma-Aldrich), chromium nitrate ($Cr(NO_3)_3$, 99% Sigma-Aldrich) were used as precursors; urea (CH_4N_2O), polyvinylpyrrolidone (PVP) and citric acid ($C_6H_8O_7$) were used as a stabilizers; distilled water and ethanol (C_2H_6O) were used as solvents.

2.2. Preparation of Pure Al_2O_3 Nanoparticles

In order to synthesize the Al_2O_3 nanoparticles *via* sol−gel method, the precursor reacts with solvent (distilled water) to form a clear solution; so, we dissolve 17.5 g of aluminium chloride hexahydrate ($AlCl_3 \cdot 6H_2O$ salt) in 100 ml of distilled water under continuous stirring at room temperature during 1 hour. Then, 5 ml of ethanol (C_2H_6O) was added to the above-mentioned solution. In this step, the temperature was increased to 70°C. After the next 5 minutes of magnetic stirrer, 8 g of polyvinylpyrrolidone (PVP) stabilizer were

added to the obtained solution. In order to obtain alumina sample in powders' form, the solutions were dried at 100°C for 24 hours to evaporate the contained water and to remove organic compounds. The resulting powders were grinded with mortar-pastel and, then, calcined in an electrical furnace at 500°C for 4 hours.

2.3. Preparation of Pure $ZnAl_2O_4$ Nanoparticles

Spinel $ZnAl_2O_4$ nanoparticles were synthesized by means of the sol–gel method involving the mixture of zinc nitrate hexahydrate $Zn(NO_3)_2 \cdot 6H_2O$ and aluminium nitrate nonahydrate $Al(NO_3)_3 \cdot 9H_2O$. Firstly, 12.5 g of $Zn(NO_3)_2 \cdot 6H_2O$ and 15 g of $Al(NO_3)_3 \cdot 9H_2O$ were dissolved in 100 ml of distilled water following the magnetic stirrer at a room temperature. The urea solution (3.75 g of CH_4N_2O in 20 ml of distilled water) has been added drop wise to the above-mentioned solution. After 3 hours of stirrer, 10 g of citric acid ($C_6H_8O_7$) were added to the zinc aluminate solution. The final product was obtained after 5 hours. The gel was dried at a temperature of 100°C in an oven for powders' synthesis. Resulting white powders were calcined at 500°C for 4 hours.

2.3. Preparation of Cr-Doped Al_2O_3 and $ZnAl_2O_4$

To synthesize the Cr-doped Al_2O_3 and Cr-doped $ZnAl_2O_4$, different quantities of chromium nitrate $Cr(NO_3)_3$ (1%, 3% and 5%) were solved in 10 ml of distilled water; afterward, chromium solution was added to the pure Al_2O_3 and $ZnAl_2O_4$ solutions, and the synthesis process was conducted similarly to the pure samples.

2.4. Characterization

The phase composition of ours synthesized matrix was analyzed by the x-ray diffraction spectrometer (MiniFlex 600 powder diffractometer with CuK_α radiation ($\lambda = 1.5406$ Å) in the range from 3° to 90°); optical properties were studied using the SHIMADZU (UV-1650-PC) double beam spectrophotometer. FT-IR spectra were recorded by using the Alpha Bruker FT-IR spectrometer.

3. RESULTS AND DISCUSSION

3.1. UV-Vis Spectroscopy

To study the effect of chromium (Cr^{3+}) impurity on the optical
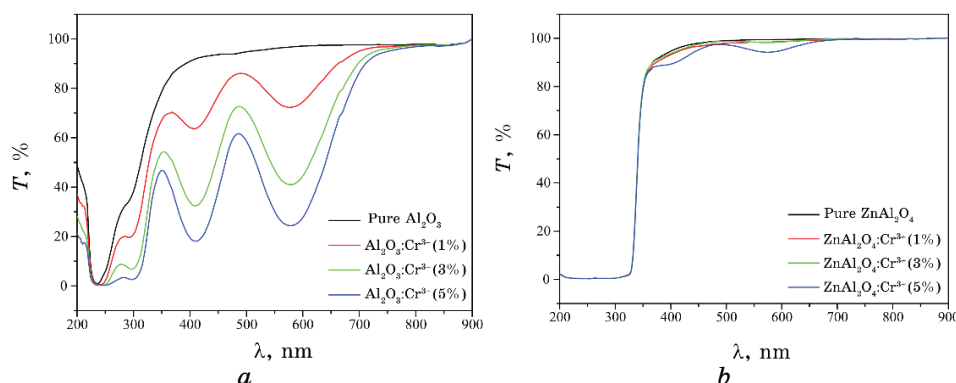
Fig. 1. UV-Vis spectra of the (*a*) Al_2O_3:Cr^{3+} and (*b*) $ZnAl_2O_4$:Cr^{3+} nanoparticles synthesized by sol−gel method and calcined at 500°C.

properties of alumina (Al_2O_3) and zinc aluminate ($ZnAl_2O_4$) synthesized by sol−gel method and calcined at 500°C, solution samples of these compounds were analysed using UV-Vis spectroscopy.

Figure 1, *a* and Figure 1, *b* show the transmittance spectra of Al_2O_3:Cr^{3+} and $ZnAl_2O_3$:Cr^{3+}, respectively. The average transmittance for the pure Al_2O_3 was above 85%, but, following the increasing in the doping concentration, two broad bands were observed in the visible wavelengths (centred at 406 nm and at 562 nm). These bands may be associated with the following *d−d* electronic transitions of Cr^{3+}: $^4A_{2g} \rightarrow {}^4T_{1g}$ (406 nm) and $^4A_{2g} \rightarrow {}^4T_{2g}$ (562 nm) according to the diagram of Shirpour *et al.* [29, 43, 44]. For the $ZnAl_2O_4$:Cr^{3+} nanoparticles, the average transmittance was above 85% in the visible region. It can be observed that the transmittance decreased with the increases of the doping concentration.

Variation of absorption coefficients of Cr-doped Al_2O_3 and Cr-doped $ZnAl_2O_4$ are presented in Fig. 2, *a*, *b*, respectively.

The relationship between the optical band-gap energy (E_g) and the absorption coefficient (α) is given by Tauc's equation [45]:

$$\alpha h\nu = \mathscr{A}\left(h\nu - E_g\right)^n,$$

where $\mathscr{A}$ is a constant and E_g is an optical band-gap of the studied sample. The exponent *n* is taken as ½, since it is direct allowed transitions. The band-gap energy (E_g) can be obtained by plotting a graph $(\alpha h\nu)^2$ versus $h\nu$ and extrapolating linear portion of the absorption edge.

The calculated band-gap by Tauc's plot for all samples is shown in Fig. 3, *a*, *b*. Obtained values of optical band-gap energy are tabulated in Table 1.
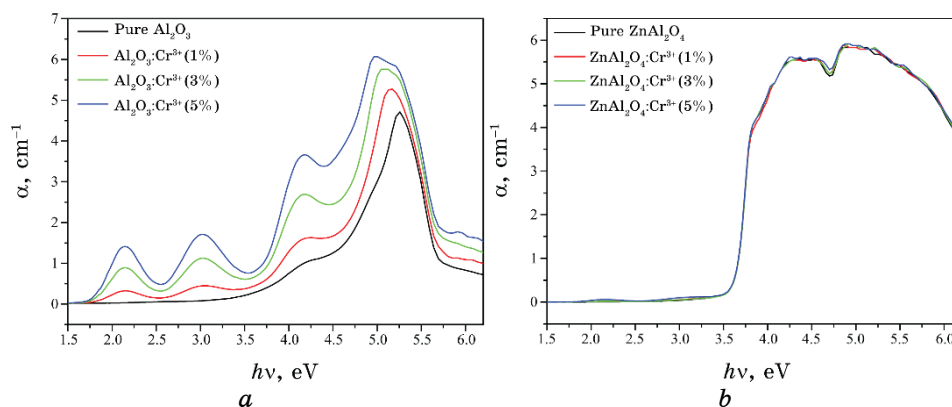
Fig. 2. Variation of absorption coefficient (α) as function of energy ($h\nu$) for the (*a*) Al_2O_3:Cr^{3+} and (*b*) $ZnAl_2O_4$:Cr^{3+} nanoparticles.
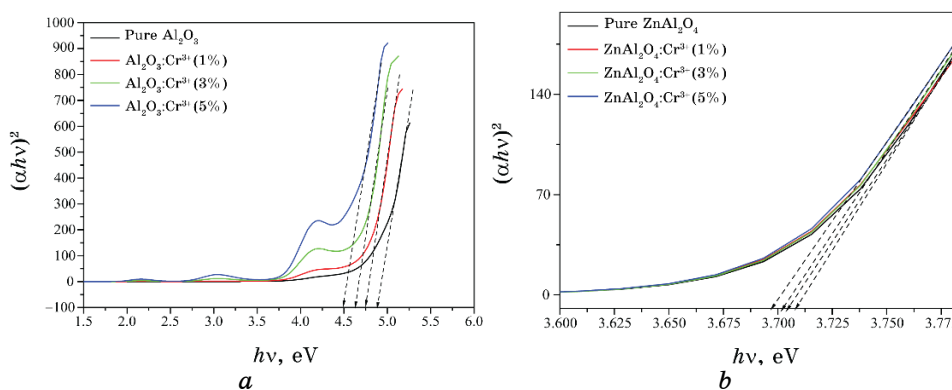
Fig. 3. Plots of $(\alpha h\nu)^2$ *versus* photon energy for the (*a*) Al_2O_3:Cr^{3+} and (*b*) $ZnAl_2O_4$:Cr^{3+} nanoparticles.

Figure 4 shows the variation of the optical band-gap energy (E_g) *versus* chromium (Cr^{3+}) concentration. It is observed that the optical band-energy decreased from 4.881 eV to 4.493 eV with increasing Cr^{3+} concentration for the Cr-doped Al_2O_3 nanoparticles. No change was observed in the optical band-gap energy for the Cr-doped $ZnAl_2O_4$ nanoparticles. We know that the band-gap is a region in energies with no allowed states. The density of states (DOS) *versus* energy depends on the chemical composition of the material; if the chemical composition is changed, at least, in principle, the DOS distribution should change. Doping is the action to add impurities; so, the chemical composition changes by doping. The change in the energy distribution of the allowed states cannot have a general rule

TABLE 1. Optical band-gap values for the $Al_2O_3:Cr^{3+}$ and $ZnAl_2O_4:Cr^{3+}$ calculated using the Tauc's equation.

Samples	E_g, eV	References
Al_2O_3	4.881	
$Al_2O_3:Cr^{3+}$ (1%)	4.756	4.06 eV [28]
$Al_2O_3:Cr^{3+}$ (3%)	4.631	
$Al_2O_3:Cr^{3+}$ (5%)	4.493	
$ZnAl_2O_4$	3.707	
$ZnAl_2O_4:Cr^{3+}$ (1%)	3.706	3.8 eV [10, 11]
$ZnAl_2O_4:Cr^{3+}$ (3%)	3.705	
$ZnAl_2O_4:Cr^{3+}$ (5%)	3.703	
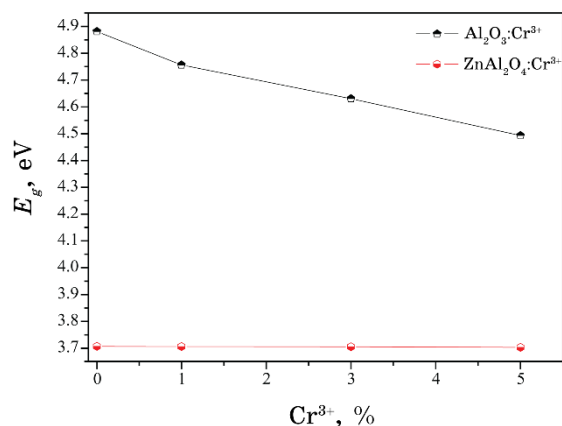
Fig. 4. Dependence of the optical band-gap energy of Cr-doped Al_2O_3 and Cr-doped $ZnAl_2O_4$ nanoparticles on Cr^{3+} concentration.

such as the band-gap will decrease after introduction of impurities. Generally, those impurities are called dopants, which create allowed shallow states in the band-gap. Shallow states have small ionisation energies; and, when the doping density is high, the dopant states generate a band. If this band is very close to the valence or conduction band edges, the band-gap will decrease.

3.2. XRD Measurements

The XRD patterns of Cr-doped Al_2O_3 and Cr-doped $ZnAl_2O_4$ obtained after calcination at 500°C are shown in Fig. 5, *a*, *b*, respectively.

As regards the XRD pattern of Al_2O_3 nanoparticles (Fig. 5, *a*), the diffraction peaks appeared at the 2θ-values of 33.23° (220),
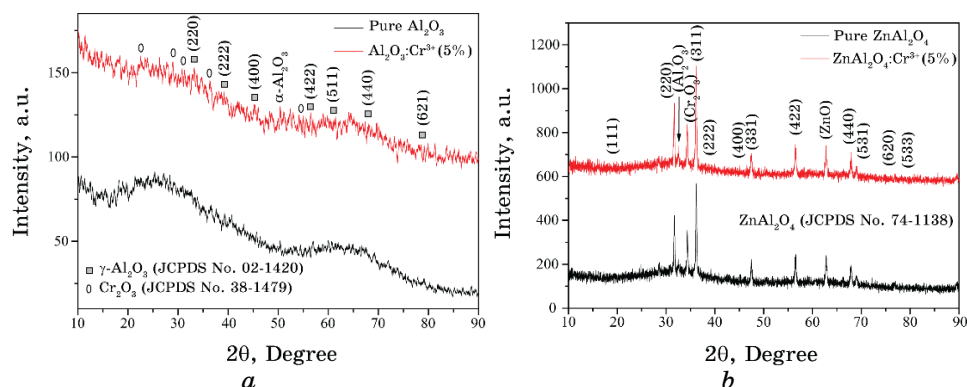
Fig. 5. XRD patterns of (*a*) $Al_2O_3:Cr^{3+}$ and (*b*) $ZnAl_2O_4:Cr^{3+}$ nanoparticles calcined at 500°C.

39.02° (222), 45.25° (400), 56.38° (422), 61.28° (511), 67.96° (440) and 78.86° (621) confirm the cubic phase of γ-Al_2O_3 with the unit cell parameter $a = 7.912$ Å. These have been coordinated with JCPDS card No. 02-1420. Some diffraction peaks have been attributed to the formation of chromium oxide Cr_2O_3 [29]. Low-intensity peak of α-Al_2O_3 was detected at the 2θ-value of 52.02°.

The diffraction peaks at 19.26° (111), 31.51° (220), 63.18° (311), 39.08° (222), 45.09° (400), 47.54° (331), 56.44° (422), 67.80° (440), 69.13° (531), 75.59° (620) and 79.82° (533) observed in Fig. 5, *b* are in agreement with JCPDS card No. 74-1138 that confirms the cubic system of $ZnAl_2O_4$ with the lattice parameter $a = 7.996$ Å and the *Fd3m* space group. Three diffraction peaks at the 2θ-values of 32.79°, 34.35° and 62.63° have been attributed to the presence of Al_2O_3, Cr_2O_3 and ZnO compounds, respectively.

Concerning the Cr-doped Al_2O_3 and $ZnAl_2O_4$ compounds calcined at 500°C, the cubic phases were obtained always. These tow observations indicated that chromium (Cr^{3+}) ions were successfully and completely incorporated into the Al_2O_3 and $ZnAl_2O_4$ crystal lattice. Comparing the atomic radius of Cr^{3+} (0.63 Å) with Al^{3+} (0.53 Å) and Zn^{2+} ions (0.74 Å) suggests that Cr^{3+} ions likely substitute Al^{3+} atoms at the octahedral sites.

The crystallites' sizes were calculated by Scherrer's equation [46] using the most intense diffraction peaks (220) for Al_2O_3 nanoparticles and (311) for $ZnAl_2O_4$ ones. Obtained sizes have been tabulated in Table 2. The crystallites' sizes were found to be in the range from 192.968 nm to 460.765 nm for $Al_2O_3:Cr^{3+}$ nanoparticles and they were found to be constant (≈ 32 nm) for $ZnAl_2O_4:Cr^{3+}$ nanoparticles. For the alumina compound, it can be seen that the size of the particles is increasing with the increase in the concentration of

TABLE 2. Crystallites' sizes for the Al_2O_3:Cr^{3+} and $ZnAl_2O_4$:Cr^{3+} obtained from XRD patterns.

Samples	2θ, °	hkl	$FWHM$, °	D, nm
Pure Al_2O_3	33.461	220	0.043	192.968
Al_2O_3:Cr^{3+} (5%)	33.340	220	0.018	460.765
Pure $ZnAl_2O_4$	36.170	311	0.257	32.545
$ZnAl_2O_4$:Cr^{3+} (5%)	36.140	311	0.256	32.688
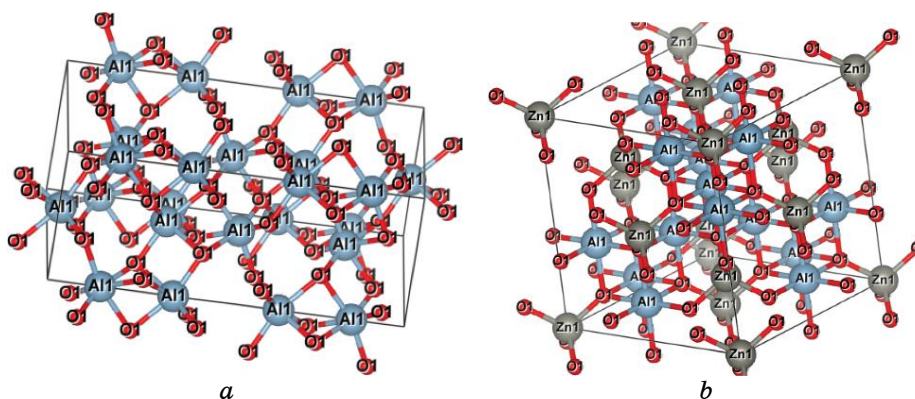
Fig. 6. Unit-cells' schemes of (*a*) Al_2O_3 and (*b*) $ZnAl_2O_4$.

chromium (Cr^{3+}) ions; this change may be explained by the difference of atomic radii of Cr^{3+} and Al^{3+} ions. No change has been observed for zinc aluminate compound because the concentration of doping impurities (Cr^{3+} ions) is very small; so, the effects on structure will be negligible.

Figures 6, *a*, *b* show the alumina (Al_2O_3) and zinc aluminate ($ZnAl_2O_4$) unit cells performed by using VESTA code.

3.3. Fourier Transform Infrared (FT-IR) Spectroscopy

The FT-IR spectra of Cr-doped Al_2O_3 and Cr-doped $ZnAl_2O_4$ nanoparticles synthesized by using the sol−gel method and calcined at the same temperature (500°C) were recorded in the wave-number range from 4000 cm^{-1} to 400 cm^{-1} and are shown in Fig. 7, *a*, *b*. The two strongly bands at around 3433 cm^{-1} and 1643 cm^{-1} have been attributed to the stretching mode of the OH^- group and the adsorption due to H_2O molecules, respectively [47, 48]. The Al−O stretching and bending modes have been characterized by two absorption bands at low energies (500−700 cm^{-1}) with peaks at 680 cm^{-1} and
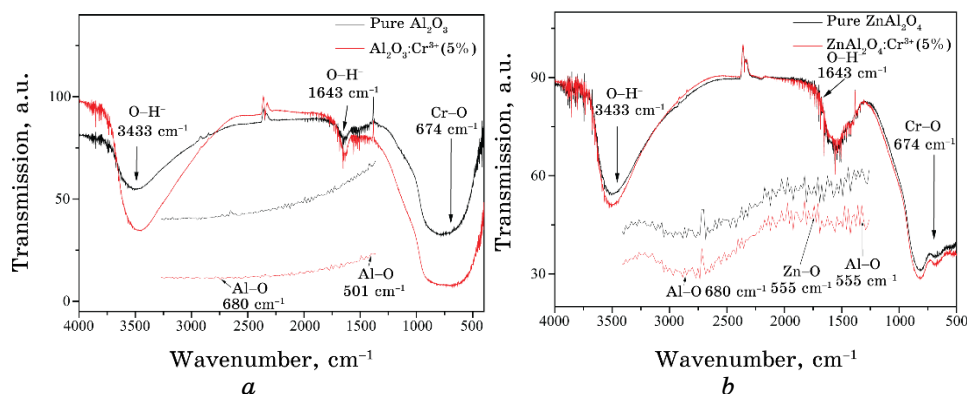
Fig. 7. FT-IR spectra of (*a*) $Al_2O_3:Cr^{3+}$ and (*b*) $ZnAl_2O_4:Cr^{3+}$ nanoparticles.

501 cm^{-1}, respectively [49−51]. Absorption band at 555 cm^{-1} was attributed to the stretching mode from Zn−O [52, 53]. The incorporation of doping (Cr^{3+}) ions in ours matrixes Al_2O_3 and $ZnAl_2O_4$ has been confirmed by the low-energy peak from Cr−O at 674 cm^{-1} [54].

4. CONCLUSIONS

In the present paper, a sol−gel synthesis method was used for preparation of Cr-doped alumina (Al_2O_3) and zinc aluminate ($ZnAl_2O_4$) nanoparticles. Obtained powders were calcined at 500°C. UV-visible (UV-Vis) spectroscopy, Fourier Transform Infrared (FT-IR) spectroscopy and x-ray diffraction (XRD) confirm that chromium (Cr^{3+}) ions have been successfully incorporated into Al_2O_3 and ZnAl2O4 crystal lattices. The optical-gap values indicate the insulator ($E_g = 4.881$ eV) and semi-conductor ($E_g = 3.707$ eV) character of Al_2O_3 and $ZnAl_2O_4$, respectively. The incorporation of chromium atoms in ours synthesized matrix has been confirmed by the FT-IR spectroscopy; it was explained by formation of Cr−O complex in both materials (with peak at 674 cm^{-1}). The XRD patterns revealed the formation of cubic structure for both $Al_2O_3:Cr^{3+}$ and $ZnAl_2O_4:Cr^{3+}$ nanoparticles. They also revealed some low-intensity peaks for α-Al2O3. The crystallite size was found to be in the range from 192.968 nm to 460.765 nm for $Al_2O_3:Cr^{3+}$ nanoparticles and it was found to be constant (≈ 32 nm) for $ZnAl_2O_4:Cr^{3+}$ nanoparticles.

ACKNOWLEDGMENTS

REFERENCES

1.   A. Aranzabal and J. L. Ayastuy, *Ind. Eng. Chem. Res.*, **42**: 6007 (2003); https://doi.org/10.1021/ie030286r
2.   A. Khodadadi, M. Farahmandjou, and M. Yaghoubi, *Mater. Res. Express*, **6**: 025029 (2019); https://doi.org/10.1088/2053-1591/aaef70
3.   B. Miranda, E. Dıáz, and S. Ordonez, *Catal. Commun.*, **7**: 945 (2006); https://doi.org/10.1016/j.catcom.2006.04.007
4.   N. Bejenaru, C. Lancelot, P. Blanchard, C. Lamonier, L. Rouleau, E. Payen, F. Dumeignil, and S. Royer, *Chem. Mater.*, **21**: 522 (2009); https://doi.org/10.1021/cm802084e
5.   M. Farahmandjou and N. Golabiyan, *J. Ceramic Proc. Res.*, **16**: 237 (2015).
6.   M. Farahmandjou and N. Golabiyan, *Transp. Phenom. Nano. Micro. Scales*, **3**: 100 (2015); https://doi.org/10.7508/TPNMS.2015.02.004
7.   P. D. Shelke and A. S. Rajbhoj, *Der Chemica Sinica*, **8**, No. 5: 482 (2017).
8.   J. A. Wang, X. Bokhimi, A. Morales, O. Novaro, and T. Lopez, *J. Phys. Chem. B*, **103**: 299 (1999); https://doi.org/10.1021/jp983130r
9.   K. N. P. Kumar, J. Tranto, J. Kumar, and J. E. Engell, *Mater. Sci. Lett.*, **15**: 266 (1996); https://doi.org/10.1007/BF00274471
10.   S. A. Mirbagheri, S. M. Masoudpanah, and S. Alamolhoda, *Optik*, **204**: 164 (2020); https://doi.org/10.1016/j.ijleo.2020.164170
11.   G. Rani, *Powder Technology*, **312**: 354 (2017); doi:10.1016/j.powtec.2017.02.040
12.   M. Tsai, Y. Chen, P. Tsai, and Y. Wang, *Thin Solid Films*, **518**: 9 (2010); https://doi.org/10.1016/j.tsf.2010.03.086
13.   M. Zawadzki, W. Staszak, F. E. Lopez-Suarez, M. J. Gomez, and A. Bueno-Lopez, *Appl. Catal. A: Gen.*, **371**: 92 (2009); https://doi.org/10.1016/j.apcata.2009.09.035
14.   V. Singh, R. P. S. Chakradhar, J. L. Rao, and D. K. Kim, *J. Lumin.*, **128**: 394 (2008); https://doi.org/10.1016/j.jlumin.2007.09.022
15.   E. M. A. Jamal, D. S. Kumar, and M. R. Anantharaman, *Bull. Mater. Sci.*, **34**: 251 (2011); https://doi.org/10.1007/s12034-011-0071-y
16.   H. Boysen, M. Lerch, A. Stys, and A. Senyshyn, *Acta Crystallogr. Sect. B Struct. Sci.*, **63**: 675 (2007); https://doi.org/10.1107/S0108768107030005
17.   L. Gong, Z. Lin, S. Ning, J. Sun, J. Shen, Y. Torimoto, and Q. Li, *Mater. Lett.*, **64**: 1322 (2010); https://doi.org/10.1016/j.matlet.2010.03.023
18.   S. N. Ude, C. J. Rawn, R. A. Peascoe, M. J. Kirkham, G. L. Jones, and E. A. Payzant, *Ceram. Int.*, **40**: 1117 (2014); https://doi.org/10.1016/j.ceramint.2013.06.112
19.   J. R. Salasin and C. Rawn, *Ceramics*, **1**: 175 (2018); https://doi.org/10.3390/ceramics1010016
20.   C. Li, D. Hirabayashi, and K. Suzuki, *Mater. Res. Bull.*, **46**: 1307 (2011); https://doi.org/10.1016/j.materresbull.2011.03.023
21.   B. Raab and H. Poellmann, *Thermochim. Acta*, **513**: 106 (2011); https://doi.org/10.1016/j.tca.2010.11.019
22.   M. M. Rashad, A. G. Mostafa, and D. A. Rayan, *J. Mater. Sci. Mater. Elec-*

tron., **27**: 2614 (2016); https://doi.org/10.1007/s10854-015-4067-z

23. W. Kerrour, A. Kabir, G. Schmerber, B. Boudjema, S. Zerkout, A. Bouabellou, and C. Sedrati, *J. Mater. Sci. Mater. Electron.*, **27**: 10106 (2016); https://doi.org/10.1007/s10854-016-5085-1

24. N. Vigneshwaran, V. Prasad, A. Arputharaj, A. K. Bharimalla, and P. G. Patil, *Nanomaterials in the Wet Processing of Textiles* (Eds. Shahid ul-Islam and B. S. Butola) (Wiley Online Library: 2018), Ch. **3**, p. 113; https://doi.org/10.1002/9781119459804.ch3

25. K. B. Kumar and P. Raji, *Recent Res. Sci. Technol.*, **3**: 48 (2011).

26. A. Samy, H. M. A. Hassan, A. E. Sherbiny, M. O. Abd-Elsamee, and M. A. Mohamed, *International Journal of Recent Scientific Research*, **6**: 4091 (2015).

27. Z. Zhu, D. Liu, H. Liu, J. Du, H. Yu, and J. Deng, *Optics Communications*, **285**: 3140 (2012); https://doi.org/10.1016/j.optcom.2012.02.084

28. M. Farahmandjou and S. Motaghi, *Optics Communications*, **441**: 1 (2019); https://doi.org/10.1016/j.optcom.2019.02.029

29. D. K. Nguyen, Q. V. Bach, B. Kim, H. Lee, C. Kang, and I. T. Kim, *Materials Chemistry and Physics*, **223**: 708 (2019); https://doi.org/10.1016/j.matchemphys.2018.11.070

30. Z. Hosseini, M. Taghizadeh, and F. Yaripour, *Journal of Natural Gas Chemistry*, **20**: 128 (2011); https://doi.org/10.1016/S1003-9953(10)60172-7

31. X. Mi, X. Zhang, X. Ba, Z. Bai, L. Lu, X. Wang, and Q. Liu, *Advanced Powder Technology*, **20**: 164 (2009); https://doi.org/10.1016/j.apt.2008.06.003

32. C. Pan, S. Y. Chen, and P. Shen, *Journal of Crystal Growth*, **310**: 699 (2008); https://doi.org/10.1016/j.jcrysgro.2007.11.089

33. A. Patra, R. E. Tallman, and B. A. Weinstein, *Optical Materials*, **27**: 1396 (2005); https://doi.org/10.1016/j.optmat.2004.10.002

34. B. Cheng, S. Qu, H. Zhou, and Z. Wang, *Nanotechnology*, **17**: 2982 (2006); https://doi.org/10.1088/0957-4484/17/12/027

35. W. Mekprasart, K. Boonyarattanakalin, W. Pecharapa, and K. N. Ishihara, *Materials Today: Proceedings*, **5**: 14126 (2018); https://doi.org/10.1016/j.matpr.2018.02.076

36. F. Z. Akika, M. Benamira, H. Lahmar, M. Trari, I. Avramova, and S. Suzer, *Surfaces and Interfaces*, **18**: 100406 (2020); https://doi.org/10.1016/j.surfin.2019.100406

37. V. Singh, N. Singh, M. S. Pathak, V. Dubey, and P. K. Singh, *Optics*, **155**: 285 (2018); https://doi.org/10.1016/j.ijleo.2017.10.167

38. Z. Han, R. Xie, Y. Song, G. Fan, L. Yang, and F. Li, *Molecular Catalysis* **477**: 110559 (2019); https://doi.org/10.1016/j.mcat.2019.110559

39. C. Z. Koepke, K. Wisniewski, M. Grinberg, and G. H. Beall, *Spectrochim. Acta Part A*, **54**: 1725 (1998); https://doi.org/10.1016/S1386-1425(98)00104-8

40. G. Dong, X. Xiao, M. Peng, Z. Ma, S. Ye, D. Chen, H. Qin, G. Deng, Q. Liang, and J. Qiu, *RSC Adv.*, **2**: 2773 (2012); https://doi.org/10.1039/C2RA00516F

41. I. Miron and I. Grozescu, *Optoelect. Adv. Mat.*, **6**: 673 (2012).

42. S. V. Motloung, F. B. Dejene, H. C. Swart, and O. M. Ntwaeaborwa, *Ceramics International*, **41**: 6776 (2015);

https://doi.org/10.1016/j.ceramint.2015.01.124

43.   M. Shirpour, M. A. Faghihi Sani, and A. Mirhabibi, *Ceram. Int.*, **33**: 1427 (2007); https://doi.org/10.1016/j.ceramint.2006.04.023

44.   H. Xuanmeng, Z. Zhenfeng, L. Hui, and F. Lu, *Rare Metal Mat. Eng.*, **45**: 1659 (2016); https://doi.org/10.1016/S1875-5372(16)30135-7

45.   J. Tauc, *The Optical Properties of Solids* (Waltham: Academic: 1966).

46.   B. D. Cullity, *Elements of X-Ray Diffraction* (Addison Wesley: 1978), p. 285.

47.   A. Gammard, O. Babaot, B. Jousseaucne, M.C. Rascle, T. Toupance, and G. Campet, *Chem. Mater.*, **12**: 3419 (2000); https://doi.org/10.1021/cm001073k

48.   Z. Zhu, X. Li, Q. Zhao, S. Liu, X. Hu, and G. Chen, *Mater. Lett.*, **65**: 194 (2011); https://doi.org/10.1016/j.matlet.2010.09.085

49.   A. A. Da Silva, A. de Souza Gonçalves, and M. R. Davolos, *Journal of Sol–Gel Science and Technology*, **49**: 101 (2009); https://doi.org/10.1007/s10971-008-1833-x

50.   P. McMillan and B. Piriou, *J. Non-Cryst. Solids*, **53**: 279 (1982); https://doi.org/10.1016/0022-3093(82)90086-2

51.   S. Mathur, M. Veith, M. Haas, H. Shen, N. Lecerf, V. Huch, S. Hüfner, R. Haberkorn, H. P. Beck, and M. Jilavi, *Journal of the American Ceramic Society*, **84**: 1921 (2001); https://doi.org/10.1111/j.1151-2916.2001.tb00938.x

52.   S. Kumar, T. Song, S. Gautam, K. Chae, S. Kim, and K. Jang, *Materials Research Bulletin*, **66**: 76 (2015); https://doi.org/10.1016/j.materresbull.2015.02.020

53.   D. Japić, M. Bitenc, M. Marinšek, and Z. C. Orel, *Materials Research Bulletin*, **60**: 738 (2014); https://doi.org/10.1016/j.materresbull.2014.09.061

54.   C. Madi, M. Tabbal, T. Christidis, S. Isber, B. Nsouli, and K. Zahraman, *Journal of Physics: Conference Series*, **59**: 600 (2007); https://doi.org/10.1088/1742-6596/59/1/128